Preprints of the 21st IFAC World Congress (Virtual)
Berlin, Germany, July 12-17, 2020

Control Allocation for Hybrid Braking Considering Dynamic Battery Behaviour

Stefan Lupberger [*,**] **Wolfgang Degel** [*,**] **Dirk Odenthal** [*]
Naim Bajcinca [**]

[*] *BMW M GmbH, Daimlerstrasse 19, 85748 Garching bei Muenchen, Germany (e-mail: Stefan.Lupberger@bmw-m.com, Wolfgang.WD.Degel@bmw-m.com, Dirk.Odenthal@bmw-m.com).*
[**] *Department of Mechatronics in Mechanical and Automotive Engineering, University of Kaiserslautern, Postfach 3049, 67663 Kaiserslautern, Germany (e-mail: naim.bajcinca@mv.uni-kl.de)*

Abstract: This work deals with the problem of maximizing energy recovery while optimizing braking capability of high-performance electric vehicles under given actuator constraints. A scalable, real-time capable concept using a complementary filter with an additional daisy chain for the control allocation between hydraulic brakes and electric motors is proposed. Furthermore, a model inversion approach that derives necessary battery limits while trying to decouple the wheel speed control loop from the protection loop of a modern battery management system is described. The hybrid braking control architecture is studied in simulation and validated in a prototype electric vehicle by highly dynamical driving manoeuvres.

Keywords: Automotive control, electric vehicles, control allocation, brake control, decoupling.

1. INTRODUCTION

With the increasing popularity of electric drives for high-performance vehicles it becomes desirable to max out the dynamic potential for this kind of drivetrains. Regarding hybrid braking, modern electric vehicles (EV) rarely exploit the fast and precise controllability of electric motors while maximizing recuperation at the same time (Ivanov et al. (2015)). The combination of both might not improve the energy balance when the driver is braking on dry roads with limited deceleration. However, it is essential for an efficient energy consumption when a significant amount of slip-controlled braking manoeuvres are performed, e.g. when driving on a race track or on icy roads.

The underlying control problem of an over-actuated system using electric motors as well as hydraulic brakes for acting on the same rotational degree of freedom has been addressed multiple times. Johansen and Fossen (2013) present an overview of different allocation approaches for over-actuated systems and their application in various branches. Ivanov et al. (2015) issue a survey of traction control and antilock braking systems for full electric vehicles including torque blending algorithms for hybrid braking such as logic-, fuzzy- and sliding-mode based variants.

Daisy chains and optimization-based methods hereby represent the most prevalent approaches. Using a daisy chain, as introduced by Adams et al. (1994) in flight control and applied to hybrid braking e.g. in Ko et al. (2015), is a pragmatic approach. Yet, in its simplest form, it is only able to maximize energy recovery and does not exploit the dynamic superiority of electric motors over electro-hydraulic brakes. In Härkegård (2004) a quadratic-programming-based problem formulation is presented which is referred to as dynamic control allocation (DCA) and considers actuator magnitude, as well as rate limits. De Castro et al. (2012) show its application for an EV in simulation. Moreover, Satzger et al. (2014) compare DCA, daisy chain and model-predictive control allocation (MPCA) for hybrid braking. Computational effort poses the main obstruction for implementation of optimization approaches on low-cost control units in modern vehicles to date. Bächle et al. (2015) show a real-time implementation of MPCA on a control prototyping platform. However, direct control of the wheel slip is omitted for complexity reduction.

In cascaded control architectures with wheel speed controllers, derived logic-based methods are used to avoid implementing the costly optimization. Rosenberger et al. (2012) try to emulate the frequency-dependent distribution of DCA using a state machine that keeps the torque of one actuator constant as long as possible and only modulates with the second one. This only facilitates either fast torque modulation using the dynamically superior electric motor or quasi-static recuperation. Solving this conflict of aims between improved wheel speed control and maximized energy recovery is the main scope of this paper.

The second contribution is the explicit consideration of dynamic battery behaviour as determinant system limitation which can interfere with the wheel speed controller in these control architectures. De Castro et al. (2012) restrict the consideration to the use of an indicator which sets the allowed regenerative braking torque to zero when the state-of-charge (SoC) reaches an upper threshold. Rajendran et al. (2018) assume a constant battery voltage and peak power in order to calculate a current limit for a deceleration manoeuvre. In this paper, a feedforward approach based on an equivalent-circuit model is introduced instead.

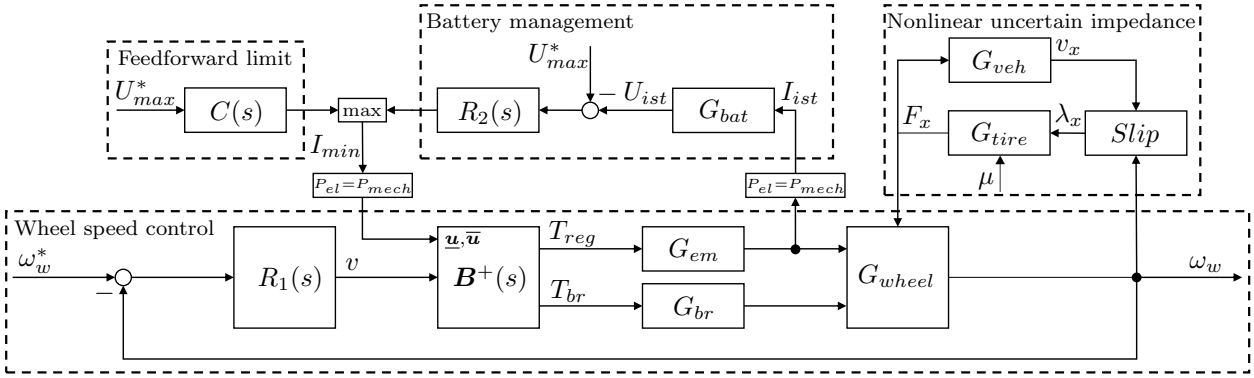

Fig. 1. Illustration of the interaction between wheel speed control loop with its controller $R_1(s)$ plus allocation $\boldsymbol{B}^+(s)$, battery protection control loop with its controller $R_2(s)$, and a proposed feedforward battery limit controller $C(s)$.

The work is structured as follows. Firstly, the identified problems of hybrid braking are introduced. Concerning these, a concept for constrained control allocation using a combination of complementary filters and daisy chains is proposed. Subsequently, the battery model and its relation to the allocation is described. This is followed by a simulative study and experimental validations in an EV.

2. PROBLEM DESCRIPTION

EVs usually have from one up to four electric motors, as well as an electro-hydraulic brake-by-wire system integrated. Using input and output valves, a selective slip control, referred to as ABS-braking, can be realised hydraulically. The allocation design is exemplified for a single degree-of-freedom (DoF) representation here. However, it is scalable to EVs with up to four electric drives.

Remark 1. Considering Fig. 1, the present paper focusses on the synthesis of the allocation $\boldsymbol{B}^+(s)$ and the feedforward battery limit controller $C(s)$, as well as therefor necessary control-oriented models for both employed actuators (G_{em},G_{br}) and the battery (G_{bat}). For the sake of brevity, the description of the wheel speed controller $R_1(s)$, which is based on Reichensdörfer et al. (2020), and the outer control loop for setpoint-speed generation is omitted. Concerning the nonlinear tire-road contact, lateral vehicle dynamics are disregarded.

2.1 Incorporated Actuators

For the control allocation synthesis the actuated torque T for both friction brakes and electric motors are approximated by first-order lags with the transfer behaviour

$$\frac{T_i}{T_i^*}(s) = \frac{1}{\tau_i s + 1}, \quad i \in \{em, br\}. \tag{1}$$

Identification for both actuators is done by means of their step response. The time constants are shown in Table 1.

Table 1. Actuator dynamics

Actuator	Time constant
Electric motor	$\tau_{em} = 0.005s$
Friction brake	$\tau_{br} = 0.030s$

Considering the significant difference in actuator dynamics, a split of the actuation effort regarding its frequency content seems reasonable for this vehicle configuration.

Problem 1. Design a real-time capable allocation concept which utilizes the superior dynamic potential of electric drivetrains for optimized tracking of a desired wheel speed ω_w^* while simultaneously maximizing energy recovery.

2.2 System Limitations

Regenerative braking is subject to multiple constraints. Crucial boundaries are voltage and current thresholds of the electric motor and the battery. Especially lithium-ion cells are sensitive to their voltage. During charging, the peak voltage U_{max} limits the minimum negative current I_{min}, while the lower boundary U_{min} prevents its voltage from dropping too low in discharging. Additionally, the cells have discharge and charge current thresholds given by C-rates. Exceeding these can harm the cell.

These boundaries determined by battery management systems are mapped to torque limitations that restrict the regenerative torque demand of either the driver or the controller. During a controlled deceleration the coupling of the battery protection and the wheel speed control loop is shown in Fig. 1. When tracking a desired wheel speed ω_w^*, the controller $R_1(s)$ can be interfered by the battery protection while handling the nonlinear tire-road contact. The simplest realisation of $R_2(s)$ is a relay that cuts the allowed current I_{min} to zero as soon as the cell voltage exceeds a threshold. This can lead to discontinuous transitions for the boundaries and has to be prevented by an appropriate realisation of the feedforward limit $C(s)$.

Problem 2. Derive dynamic torque boundaries for a constrained control allocation, resulting from battery voltage and current constraints that circumvent the link between the control loops for battery protection and wheel speed.

3. CONTROL ALLOCATION

Assuming linear actuator models, the allocation problem is described by

$$\boldsymbol{B}\boldsymbol{u} = \boldsymbol{v}. \tag{2}$$

The control effectiveness matrix $\boldsymbol{B} \in \mathbb{R}^{k\times m}$ relates the virtual control input $\boldsymbol{v} \in \mathbb{R}^k$ to the real input $\boldsymbol{u} \in \mathbb{R}^m$. For an over-actuated system, $\boldsymbol{B}$ is assumed to possess the rank k and $m > k$. With the presence of actuator constraints, the problem is augmented by the component-wise relation

$$\underline{\boldsymbol{u}} \leq \boldsymbol{u} \leq \overline{\boldsymbol{u}}. \tag{3}$$

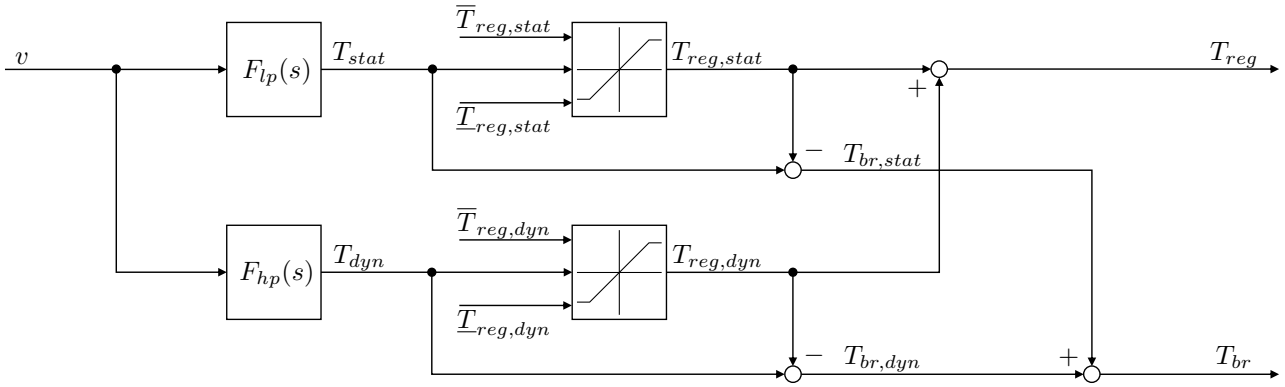

Fig. 2. Structure of the proposed control allocation concept with complementary low-pass (F_{lp}) and high-pass filters (F_{hp}) as well as additional daisy chains leading to the regenerative (T_{reg}) and friction brake torque requests (T_{br}).

For hybrid braking $k = 1$ and $m = 2$, resulting in

$$(B_{reg}\ B_{br}) \begin{pmatrix} T_{reg} \\ T_{br} \end{pmatrix} = v, \tag{4}$$

subject to

$$\begin{pmatrix} \max(\underline{T}_{em}, \underline{T}_{bat}) \\ \underline{T}_{br} \end{pmatrix} \leq \begin{pmatrix} T_{reg} \\ T_{br} \end{pmatrix} \leq \begin{pmatrix} \min(\overline{T}_{em}, \overline{T}_{bat}) \\ 0 \end{pmatrix}, \tag{5}$$

with the torque limits being $\underline{T}_{em}, \underline{T}_{bat}, \underline{T}_{br} \leq 0$ and $\overline{T}_{em}, \overline{T}_{bat} \geq 0$. In order to deduce a real-time allocation concept from the optimization approach, a brief description of DCA is given.

3.1 Dynamic Control Allocation

The problem of DCA, according to Härkegård (2004), is described by the time-discrete optimization problem

$$\Omega = \arg \min_{\underline{\boldsymbol{u}} \leq \boldsymbol{u} \leq \overline{\boldsymbol{u}}} \|\boldsymbol{W}_v(\boldsymbol{B}\boldsymbol{u} - \boldsymbol{v})\|_2, \tag{6}$$

$$\boldsymbol{u} = \arg \min_{\boldsymbol{u} \in \Omega} \|\boldsymbol{W}_1(\boldsymbol{u} - \boldsymbol{u}_s)\|_2^2 + \|\boldsymbol{W}_2(\boldsymbol{u} - \boldsymbol{u}_{t-1})\|_2^2. \tag{7}$$

$\boldsymbol{W}_1$ affects the tracking of a desired steady state control input $\boldsymbol{u}_s$, whereas $\boldsymbol{W}_2$ penalizes the change in control input compared to the input at the previous time step $\boldsymbol{u}_{t-1}$. Therefore, $\boldsymbol{W}_2$ has an effect on the frequency split of v onto actuators with different dynamics. $\boldsymbol{W}_v$ can be used to prioritize between different components of v.

Härkegård (2004) shows that the unconstrained problem for two actuators is solved explicitly by a complementary filter with fast changing portions of $\boldsymbol{v}$ being promoted to the dynamically more capable actuator. This characteristic of DCA is utilized as a starting point for the alternative control allocation concept.

3.2 Complementary Filter for Frequency Split

Since the dynamics of the brake-by-wire system are slower, it is desirable to shift actuating torques in the higher frequency range to the electric drivetrain. To perform this frequency split, the first order low- and high-pass filters

$$F_{lp}(s) = \frac{1}{\tau_{cf} s + 1}, \tag{8}$$

$$F_{hp}(s) = \frac{\tau_{cf} s}{\tau_{cf} s + 1}, \tag{9}$$

are used. This complementary filter holds the relation $F_{lp}(s) + F_{hp}(s) = 1$ which ensures that (2) isn't violated.

Alternatively, instead of adapting weight matrices in (7) for choosing τ_{cf}, classical methods for determining the design parameter can be used, too. Having modelled the control loop, criteria for performance, robustness and stability of the wheel speed control can be attempted to achieve, e.g. using loop shaping (Åström and Murray (2008)). The requirements are tried to be met by adapting τ_{cf} in the simplified case of an unconstrained allocation when propagating low-pass filtered torque requests to the brakes and fast portions to the electric drive. The high-pass fraction can then be interpreted as control effort that only the faster actuator is able to satisfactorily realize.

3.3 Daisy-Chain for Desired Steady-State

Given that the high-pass filtered content oscillates around a stationary value of zero, directly feeding this portion to the electric drive and low-pass content simply to the brakes does not optimize the recovered energy but just the system's dynamic response. Therefore, inspired by the first term in (7) which attempts stationary allocation, a downstream daisy-chain is added that prioritizes regenerative over hydraulic braking for the stationary as well as for the transient part up to static and dynamic limits. The resulting allocation structure, shown in Fig. 2, is

$$T_{stat} = F_{lp}(s)v = \frac{1}{\tau_{cf} s + 1} v, \tag{10}$$

$$T_{dyn} = F_{hp}(s)v = \frac{\tau_{cf} s}{\tau_{cf} s + 1} v, \tag{11}$$

$$\begin{aligned} T_{reg} = \min(\max(T_{stat}, \underline{T}_{reg,stat}), \overline{T}_{reg,stat}) + \\ \min(\max(T_{dyn}, \underline{T}_{reg,dyn}), \overline{T}_{reg,dyn}), \end{aligned} \tag{12}$$

$$\begin{aligned} T_{br} = T_{stat} - \min(\max(T_{stat}, \underline{T}_{reg,stat}), \overline{T}_{reg,stat}) + \\ T_{dyn} - \min(\max(T_{dyn}, \underline{T}_{reg,dyn}), \overline{T}_{reg,dyn}). \end{aligned} \tag{13}$$

The terms static and dynamic denote slow and fast fractions in this context. Required static and dynamic limits for the regenerative braking torques are discussed next.

3.4 Static and Dynamic Constraints

The boundaries must meet two properties. Firstly, since both T_{stat} and T_{dyn} are preferentially transcribed to the electric drivetrain, the sum of both fractions must not be less than the total negative regenerative torque limit, i.e.

$$\underline{T}_{reg,stat} + \underline{T}_{reg,dyn} \geq \underline{T}_{reg}. \tag{14}$$

Secondly, the quasi-static actuator boundaries should not change faster than T_{stat}. This can be achieved by computing $\underline{T}_{reg,stat}$ using the same $F_{lp}(s)$ as in (10). Additionally, in order to attain a high disturbance rejection, a torque allowance $\Delta < 0$ is introduced which tries to always facilitate the realization of T_{dyn} with the dynamically superior electric drive. This leads to the static constraint

$$\underline{T}_{reg,stat} = F_{lp}(s)\underline{T}_{reg} - \Delta. \tag{15}$$

Assuming equality in (14), the dynamic boundary is

$$\underline{T}_{reg,dyn} = (1 - F_{lp}(s))\underline{T}_{reg} + \Delta = F_{hp}(s)\underline{T}_{reg} + \Delta. \tag{16}$$

It can be seen that this approach corresponds to a complementary filtering of the torque limits.

Remark 2. Alternatively, it is also possible to use

$$\underline{T}_{reg,dyn} = \underline{T}_{reg} - T_{reg,stat} + \Delta, \tag{17}$$

with the negative torque $T_{reg,stat} \geq F_{lp}(s)\underline{T}_{reg} - \Delta$ as dynamic boundary. This can increase the dynamic potential when stationary recuperation is not (yet) fully utilized for example at the beginning of a braking manoeuvre.

4. BATTERY MODEL AND LIMITS

The derivation of necessary actuator boundaries is exemplified for the battery limitations. These often represent the main obstruction for regenerative braking, especially for high SoC. The aim is to design a feedforward controller $C(s)$ for the minimum allowable current by model inversion, which prevents the cell voltage from exceeding its limits and avoids formerly described coupling. Initially, an equivalent-circuit battery model (ECM) is described.

4.1 Equivalent-Circuit Model

Battery cells show different dynamic behaviour on various time scales. This paper focusses on their short-term dynamic behaviour. Changes occurring over lifetime are neglected. For this purpose, an ECM consisting of a resistor in series with a parallel RC element, in literature often referred to as Thevenin battery model (Salameh et al. (1992), Gao et al. (2002), Chan (2000)) and shown in Fig. 3, is contemplated.

The transfer behaviour in the frequency domain results in

$$U(s) = U_{OCV} - R_i I(s) - \frac{R_1}{(R_1 C s + 1)} I(s). \tag{18}$$

Positive currents relate to discharging while negative ones correspond to charging. The parameters R_i, R_1 and C can differ for charging and discharging and strongly depend on the SoC and the cell temperature. Therefore, the battery is modelled as a linear parameter-varying system with its

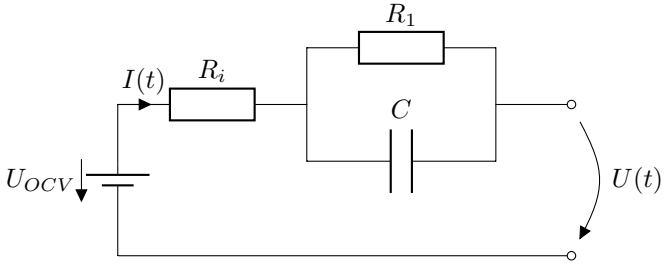

Fig. 3. Equivalent circuit model for the battery cell.

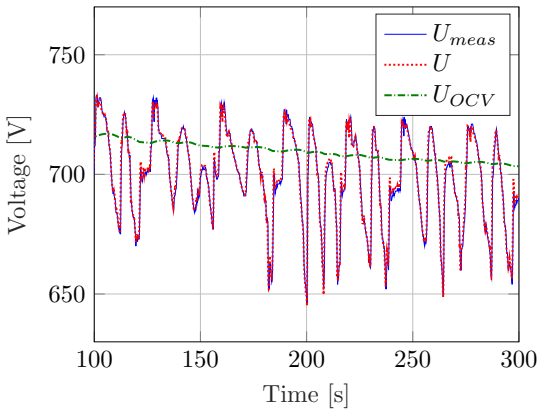

Fig. 4. Match of modelled and measured battery voltage.

parameters identified by cell tests in order to facilitate model inversion through a precise representation. Fig. 4 shows the accurate match of the model with the sensed voltage during fast driving.

The dynamic voltage behaviour resulting from the resistors and the capacity can be described by the transfer function

$$G_{bat}(s) = \frac{U_{OCV} - U(s)}{I(s)} = \frac{R_i R_1 C s + R_i + R_1}{R_1 C s + 1}, \tag{19}$$

with the battery current $I(s)$ as the system's input.

4.2 Open-Circuit Voltage

In general, the open-circuit cell voltage (OCV) U_{OCV} is a nonlinear function of the electric charge, i.e. the SoC. For the given cell, this characteristic is determined on a test rig using small charge and discharge rates. While stressing the battery, its OCV and SoC cannot be measured but need to be estimated. Piller et al. (2001) present an overview of different methods for determination of the SoC. Given the possibility of accurate current measurement for the employed battery, a combination of ampere hour counting combined with recalibration during standstill is used.

Ampere hour counting is based on the integrated withdrawn and returned current and can be described by

$$SoC(t) = SoC(t_0) + \int_{t_0}^{t} \frac{I(t)}{Q_{bat}} \mathrm{d}t, \tag{20}$$

where Q_{bat} is the rated battery capacity. The initial value $SoC(t_0)$ is determined by voltage measurement during standstill when no current is drawn or supplied, combined with the inverse characteristic relation of OCV and SoC.

Assumption 1. Compared to the voltage dynamics in (19), changes of U_{OCV} are significantly slower. This can also be seen in Fig. 4. Therefore, the OCV is assumed to be constant during a single brake action.

4.3 Feedforward Limit through Model Inversion

Given the quasi-static cell OCV and the cut-off voltage U_{max}, their difference describes the limit for the dynamic over-voltage. By inverting (19), which results in

$$G_{bat}^{-1}(s) = \frac{R_1 C s + 1}{R_i R_1 C s + R_i + R_1}, \tag{21}$$

it is possible to derive the minimum allowable charging current for the battery not to reach its voltage limit:

$$I_{min}(s) = \frac{R_1 C s + 1}{R_i R_1 C s + R_i + R_1}(U_{OCV} - U_{max}). \quad (22)$$

From (22), it can be seen that, given the voltage across an ideal capacitor is initially zero, it is possible to allow higher charging currents in the initial braking phase. As the current across the capacitor decays exponentially and the over-voltage rises, the current limit I_{min} decreases.

Remark 3. Battery packs for electric vehicles are composed of many cells interconnected in series and parallel. Under real conditions their open-circuit voltages can differ. Therefore, a worst-case consideration is proposed which uses the cell with the highest OCV for determining I_{min}.

4.4 Resulting Torque Limits for Control Allocation

Since the controller provides torque commands, it is necessary to translate the current limits into torque constraints by equating electrical and mechanical power

$$P_{el} = U_{lim} I_{lim} = \underline{T}_{bat} \omega_w = P_{mech}. \quad (23)$$

Efficiency factors are omitted. The current limit I_{lim} is given by the maximum of I_{min} resulting from voltage constraints and the C-rate charge current threshold mentioned in Section 2.2, which is dependent on the specific cell. In order to calculate the minimum electrical power, the maximum voltage U_{lim} that would result if the battery pack was charged with I_{min} is determined considering (18).

Instead of directly using the wheel speed sensors, the desired value ω_w^*, derived from a slip setpoint λ_x^*, is taken for the conversion to avoid copying the rotational wheel dynamics into the torque boundaries. With the longitudinal slip defined by

$$\lambda_x = \frac{\omega_w r_{dyn} - v_x}{\max(|\omega_w r_{dyn}|, |v_x|)}, \quad (24)$$

where r_{dyn} denotes the dynamical tire circumference, and assuming a constant λ_x^*, the desired wheel speed during braking results in

$$\omega_w^* = \frac{v_x}{r_{dyn}(1 - \lambda_x^*)}. \quad (25)$$

The total negative wheel torque threshold for regenerative braking resulting from charge limits is therefore given by

$$\underline{T}_{bat} = \frac{U_{lim} I_{lim} r_{dyn}(1 - \lambda_x^*)}{v_x}. \quad (26)$$

Analogously, a positive torque limit for discharge $\overline{T}_{bat}$ can be derived by minimum voltage and maximum current.

5. CONCEPT VALIDATION

5.1 Numerical Simulation

A closed-loop simulation with the wheel speed controller for anti-lock braking and a quarter car model given by

$$\dot{\omega}_w = \frac{1}{J_w}(T_{reg} + T_{br} - F_x(\lambda_x, \mu, F_z) r_{dyn}), \quad (27)$$

$$\dot{v}_x = \frac{1}{m}(F_x(\lambda_x, \mu, F_z) - F_w), \quad (28)$$

with the wheel moment of inertia J_w, vehicle mass m, air resistance force F_w, tire force F_x and the vertical load of the wheel F_z is performed. Its tire force F_x is modelled by Pacejka's magic formula. A qualitative numerical simulation is exerted with a sample time of $1ms$.

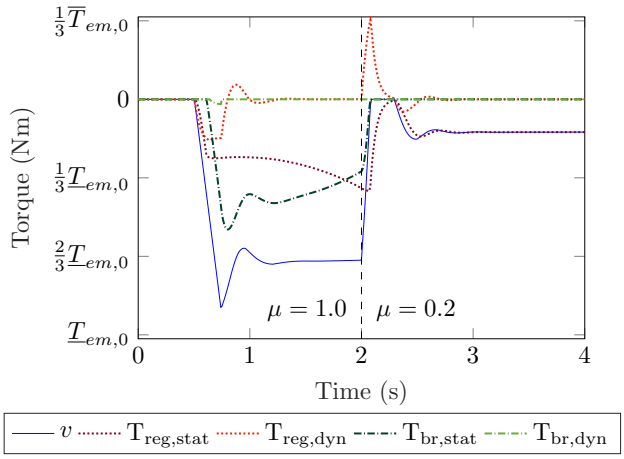

Fig. 5. Torque shares for simulated emergency braking.

An emergency braking on initially dry road with a friction coefficient $\mu = 1.0$ is simulated, with the driver applying the brakes at an initial speed of $v_{x,0} = 38\frac{m}{s}$. After two seconds the friction coefficient drops to $\mu = 0.2$ which represents an icy surface. The SoC for the cell with the highest OCV is assumed to be $SoC_{max} = 77\%$. The complementary filter time constant is chosen to be $\tau_{cf} = 60$ms for the given actuator characteristics.

Fig. 5 illustrates the virtual control input v for the front axle and the shares for hydraulic brakes and electric drivetrain. The torques are specified in relation to the symmetric motor torque limit in base speed range $\underline{T}_{em,0}$. At initial brake application, there is a negative dynamic torque shifted to the electric motors in order to quickly build deceleration. Upon controller activation, the fast dynamics of the motors are used to prevent excessive wheel slip by quickly decreasing torque. This also applies for the sudden change of friction with a positive spike of $T_{reg,dyn}$ rapidly reducing the overall torque request T_{reg}. The slowly changing fraction $T_{reg,stat}$ is limited by the low-pass filtered battery boundary which raises with decreasing velocity as emanating from (26). The friction brake torque request is changing slowly except for a minor dynamic portion during initial deceleration. This could be prevented by a higher torque allowance, which would reduce stationary recuperation, or if Δ was adaptive.

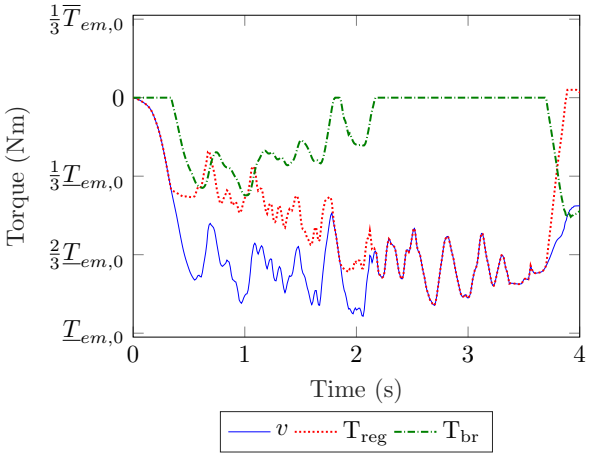

Fig. 6. Torque shares for experimental emergency braking.

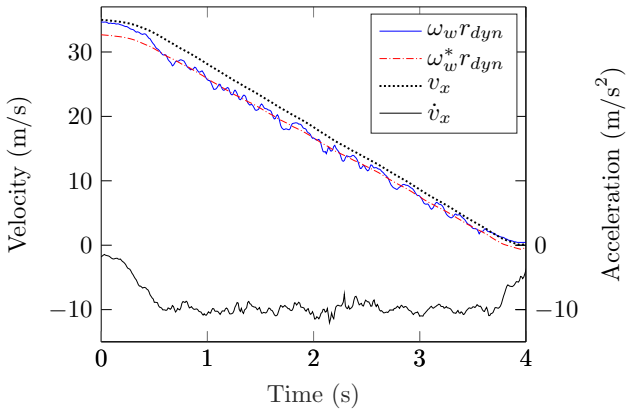

Fig. 7. Wheel velocities as well as vehicle speed and acceleration for straight-line emergency braking.

5.2 Experimental Evaluation

The control concept is implemented on an embedded rapid control prototyping platform with a cycle time of 1ms and equal parametrization for experimental validation. Fig. 6 shows the front axle actuator torques for emergency braking on dry tarmac. Below $v_x < 16.5\frac{\text{m}}{\text{s}}$ the deceleration is actuated by the electric motors only. Close to standstill, regenerative braking is phased out and counterbalanced by the friction brakes. The associated controlled mean front wheel speed ω_w in Fig. 7 illustrates reliable tracking of ω_w^* with hybrid actuation while recuperating. The unfiltered acceleration $\dot{v}_x$ indicates high mean deceleration enhancing performance and safety through short stopping distances.

Fig. 8 displays the energy balance for high performance tests on a race track. The net consumption E_{net} is the difference of consumed and regenerated energy given by $E_{consumed} = \int_{t_0}^{t_{end}} U(t)I(t)\mathrm{d}t$ for $I(t) > 0$ and $E_{recuperated} = \int_{t_0}^{t_{end}} U(t)I(t)\mathrm{d}t$ for $I(t) < 0$, respectively. Despite using the motors for optimized tracking control, energy recovery $\eta = (1 - E_{net}/E_{consumed}) \cdot 100\% > 35\%$ is achieved without harming the battery, too, showing that the Problems 1 and 2 can be solved.

6. CONCLUSION

Having shown a real-time allocation for improved wheel speed control while charging a battery at its limit during braking, it is important to recognize that the concept is scalable to any battery, controller and actuator configuration by adjusting few parameters. Further research will focus on analysis of the concept, adaptive design parameters for $\boldsymbol{B}^+(s)$ and consideration of elastic drivetrains.

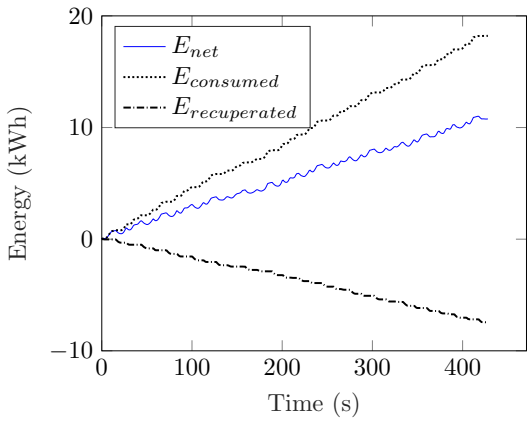

Fig. 8. Energy balance for high-performance racetrack test.

REFERENCES

Adams, R.J., Buffington, J.M., Sparks, A.G., and Banda, S.S. (1994). *Robust Multivariable Flight Control*. Springer-Verlag, London.

Åström, K.J. and Murray, R.M. (2008). *Feedback Systems: An Introduction for Scientists and Engineers*. Princeton University Press.

Bächle, T., Graichen, K., Buchholz, M., and Dietmayer, K. (2015). Model predictive control allocation in electric vehicle drive trains. *IFAC-PapersOnLine*, 48(15), 335–340.

Chan, H.L. (2000). A new battery model for use with battery energy storage systems and electric vehicles power systems. In *2000 IEEE Power Engineering Society Winter Meeting*, 470–475. Singapore.

De Castro, R., Araújo, R.E., Tanelli, M., Savaresi, S.M., and Freitas, D. (2012). Torque blending and wheel slip control in EVs with in-wheel motors. *Vehicle System Dynamics*, 50(sup1), 71–94.

Gao, L., Liu, S., and Dougal, R.A. (2002). Dynamic lithium-ion battery model for system simulation. *IEEE Trans. Compon. Packag. Technol.*, 25(3), 495–505.

Härkegård, O. (2004). Dynamic control allocation using constrained quadratic programming. *Journal of Guidance, Control, and Dynamics*, 27(6), 1028–1034.

Ivanov, V., Savitski, D., and Shyrokau, B. (2015). A survey of traction control and antilock braking systems of full electric vehicles with individually controlled electric motors. *IEEE Trans. Veh. Technol.*, 64(9), 3878–3896.

Johansen, T.A. and Fossen, T.I. (2013). Control allocation - a survey. *Automatica*, 49(5), 1087–1103.

Ko, J., Ko, S., Son, H., Yoo, B., Cheon, J., and Kim, H. (2015). Development of brake system and regenerative braking cooperative control algorithm for automatic-transmission-based hybrid electric vehicles. *IEEE Trans. Veh. Technol.*, 64(2), 431–440.

Piller, S., Perrin, M., and Jossen, A. (2001). Methods for state-of-charge determination and their applications. *Journal of Power Sources*, 96(1), 113–120.

Rajendran, S., Spurgeon, S., Tsampardoukas, G., and Hampson, R. (2018). Intelligent sliding mode scheme for regenerative braking control. *IFAC-PapersOnLine*, 51(25), 334–339.

Reichensdörfer, E., Odenthal, D., and Wollherr, D. (2020). On the stability of nonlinear wheel-slip zero dynamics in traction control systems. *IEEE Trans. Control Syst. Technol.*, 28(2), 489–504.

Rosenberger, M., Uhlig, R., Koch, T., and Lienkamp, M. (2012). Combining regenerative braking and antilock braking for enhanced braking performance and efficiency. *SAE Technical Paper 2012-01-0234*.

Salameh, Z.M., Casacca, M.A., and Lynch, W.A. (1992). A mathematical model for lead-acid batteries. *IEEE Transactions on Energy Conversion*, 7(1), 93–98.

Satzger, C., De Castro, R., and Bünte, T. (2014). A model predictive control allocation approach to hybrid braking of electric vehicles. In *2014 IEEE Intelligent Vehicles Symposium Proceedings*, 286–292. Dearborn, MI.